DOI: 10.15244/pjoes/210104

ONLINE PUBLICATION DATE: 2025-10-29

Original Research

Characteristics Analysis of Spatiotemporal Precipitation Variability in the Middle Yellow River Basin

Yu Zhansheng, Luo Mingjie°*

School of Geographic Information and Tourism, Chuzhou University, Chuzhou, China

Received: 14 April 2025 Accepted: 31 August 2025

Abstract

To conduct a comprehensive investigation into the spatiotemporal variability characteristics of precipitation within the middle Yellow River basin, elucidate the interrelationships between precipitation and key environmental factors, and assess the spatial heterogeneity of precipitation patterns. The Mann-Kendall test, Pettitt test, and Morlet wavelet analysis were employed to investigate the temporal characteristics of a 67-year (1956-2022) annual precipitation series derived from 15 monitoring stations in the Middle Yellow River Basin. The nonparametric Kruskal-Wallis H test was used to evaluate whether precipitation exhibited significant differences across these stations. Additionally, spatial autocorrelation analysis using Moran's I was conducted based on multi-year mean annual precipitation data from 230 counties/districts within the same region, to examine the clustering patterns of precipitation distribution. The results indicated that increasing precipitation trends were detected in the northern and southwestern portions of the Middle Yellow River Basin, while the remaining areas exhibited a predominant decreasing trend, though all trends were statistically non-significant $(\alpha = 0.05)$. Statistically significant trend abrupt change points in the time series primarily occurred in 1978, 2003, and 2020 at some stations. The Pettitt test indicated that the mean annual precipitation across the 15 stations showed no significant change point over time. The wavelet analysis revealed three predominant temporal scales in the study area: 5-10, 15-30, and 30-55 years, while the wavelet variance plot identified three dominant periodicities centered at approximately 10, 44, and 56 years. Heterogeneity testing demonstrated that annual precipitation differences among the 15 stations increased with latitudinal distance along the north-south transect. The global Moran's I value of 0.5533 (p<0.05) indicated significant positive spatial autocorrelation in annual precipitation across the Middle Yellow River Basin. Local Moran's I analysis revealed distinct spatial clustering patterns: high-high clusters were predominantly concentrated in the southern region, while low-low clusters aggregated in the northern and partial southwestern areas, with no significant spatial autocorrelation observed in the central zone. Although vegetation restoration in the Middle Yellow River Basin has reduced erosion, more water resources have been consumed in the process due to no significant changes in precipitation,

°ORCID iD: 0009-0009-9217-908X

^{*}e-mail: minjayro@163.com

which may increase the regional water ecological security risks. These findings provide important theoretical references for optimizing water resource allocation in the Yellow River Basin, supporting ecological conservation and sustainable development.

Keywords: middle yellow river basin, precipitation, spatiotemporal analysis, Mann-Kendall test, wavelet analysis

Introduction

As a pivotal component of climate systems, precipitation critically regulates hydrological processes including river discharge dynamics, vegetation succession, soil erosion mechanisms, and regional ecological stability [1-3]. Its spatiotemporal patterns fundamentally determine agricultural irrigation requirements, industrial water allocation strategies, and domestic water security, thereby governing integrated water resources management at regional scales. Contemporary climate observations reveal significant global alterations in precipitation regimes, particularly manifested through intensified extreme events under warming scenarios [4]. These hydrological extremes increasingly exacerbate drought-flood alternations, presenting unprecedented challenges to vegetation resilience and spatial reorganization. Notably, extreme precipitation exerts divergent ecological controls, suppressing aboveground net primary productivity (ANPP) in mesic ecosystems while enhancing it in xeric environments, with plant-available water acting as the primary mediator of these responses [5]. In the driver analysis of Normalized Difference Vegetation Index (NDVI) variations within the Huangshui River Basin during 2000-2018, both cumulative precipitation and effective cumulative precipitation exhibited positive correlations with NDVI changes, with correlation coefficients reaching 86.52% and 86.18% respectively. This hydrological pattern reveals a pronounced positive relationship between vegetation growth and precipitation dynamics [6]. The frequent occurrence of extreme precipitation will also greatly affect the growth of vegetation, leading to an increase in the frequency of droughts or floods.

The agricultural impacts of precipitation variability are particularly pronounced. Fu et al. demonstrated that significant yield reductions in Chinese rice production over two decades were due to rainfall extremes [7]. Regional analyses reveal distinct spatial vulnerability patterns: northwestern, northern, and northeastern China exhibit heightened drought sensitivity, contrasting with flood predisposition in eastern/southeastern regions [8]. This geographic coherence between irrigation demand anomalies and precipitation extremes underscores their agricultural implications, particularly in major production zones like the Yellow River Basin [9]. Similar precipitation-vegetation correlations emerge in critical ecotones like China's Loess Plateau, where moisture availability directly controls vegetation coverage [10].

Precipitation-runoff interactions demonstrate marked regional specificity. In the analysis of water-sediment variation characteristics in China's Ganjiang River Basin from 1958 to 2019, the correlation coefficient between precipitation and runoff approached 100%, indicating precipitation as the primary driver of runoff variation, with a pronounced positive correlation observed between the two variables [11]. Spatiotemporal heterogeneity is further evidenced by contrasting continental-scale patterns: most western/southwestern US regions show decreasing annual precipitation, while northern areas and the Great Plains exhibit increasing trends, accompanied by growing proportions of heavy rainfall events [12]. In northern China, concentrated precipitation patterns prevail, with maximum 4-month accumulations constituting 70-80% of annual totals, compared to 50-65% in southern regions [13]. Summer precipitation in China exhibited an increasing trend from the early 20th century to the 1950s, followed by a decreasing trend during the 1960s-1970s, and renewed increases from the 1980s to 2010. In terms of spatial distribution, precipitation exhibits a "five-layer sandwich structure" along the northwest-southeast axis, and its spatial distribution is characterized by an alternating ascending-descending pattern (ascending - descending - ascending - descending - ascending) [14].

The Yellow River, characterized by its high sedimentladen runoff, has undergone substantial hydrological changes in recent decades due to the combined effects of global climate change and anthropogenic activities, with both runoff and sediment load exhibiting precipitous declines [15, 16]. During the period from 2002 to 2019, both the annual mean and total sediment loads in the Yellow River Basin demonstrated a persistent declining trend, which has positively contributed to the ecological equilibrium and fluvial system stability of the river [17]. Hydrological variations in the river's headwater region critically influence water availability throughout the entire basin. Hou et al. conducted a comprehensive analysis of temporal patterns in precipitation [18], temperature, evapotranspiration, and runoff during 1958-2017, revealing a 14% significant reduction in runoff during 1989-2017 compared to the 1958-1988 baseline period. Spectral analysis identified 4- and 8-year periodicities in both precipitation and runoff during 1958-1988, which shifted to 6-year cycles in 1989-2017. Notably, the latter period exhibited intensified biennial oscillations in precipitation and emerging 3-year cycles in runoff variations. These hydrological changes appear climatically consistent when contextualized with observed increases in vegetation coverage and the

impacts of industrial expansion across the basin [19, 20]. The middle reaches of the Yellow River Basin feature a fragile ecological environment, where vegetation dynamics have undergone significant transformations under the combined pressures of climate change and anthropogenic activities [21]. As a sensitive responder to global climate change, this region exhibits pronounced vulnerability in key ecosystem services, particularly soil-water conservation and carbon sequestration [22].

This investigation targets the middle reaches of the Yellow River Basin, synthesizing 67-year annual precipitation records (1956-2022) from 15 meteorological stations with multi-decadal mean precipitation datasets 230 county-level administrative units. spanning Through integrated application of Mann-Kendall trend analysis with abrupt change detection, the Pettitt test for mean-shift identification, Morlet wavelet analysis, nonparametric statistical methods Kruskal-Wallis H Test, and spatial autocorrelation analysis Moran's I, this study systematically analyzed (1) temporal characteristics of annual precipitation, including trends, abrupt change points (covering both trend-breaks and mean shifts), and periodicity, as well as (2) spatial characteristics, including heterogeneity and spatial autocorrelation in this study region. The multi-scale analytical framework bridges station observations with regional hydrological responses, enabling comprehensive characterization of precipitation regimes across different spatial resolutions. This study provides critical insights for guiding waterresource management and conservation strategies in the Yellow River Basin. Moreover, precipitation variability

is intricately linked to climatic drivers-including temperature anomalies, atmospheric circulation modes, and topographic controls. The identified precipitation trends thus establish a benchmark for examining concurrent changes in other environmental variables and open new avenues for future research.

Materials and Methods

Study Area

The middle reach of the Yellow River Basin extends from Hekou Town in Inner Mongolia to Taohuayu in Henan Province, spanning 1,206.4 km and covering a drainage area of 344,000 km², which accounts for approximately 43.3% of the entire Yellow River Basin (Fig. 1). This segment traverses multiple provinces, including Inner Mongolia, Shanxi, and Shaanxi, located in the northwestern and central regions of China within the mid-latitude zone. Due to its critical role in water resource management and sediment transport, the middle reach holds strategic geographical significance [23]. Geomorphologically, this region is dominated by the Loess Plateau, situated in a transitional climatic zone between arid and humid regions of China. The area is characterized by semi-arid conditions, with precipitation predominantly concentrated during the summer months (June to August). The mean annual precipitation ranges from 400 to 900 mm, reflecting significant spatial climatic variability across the basin [24].

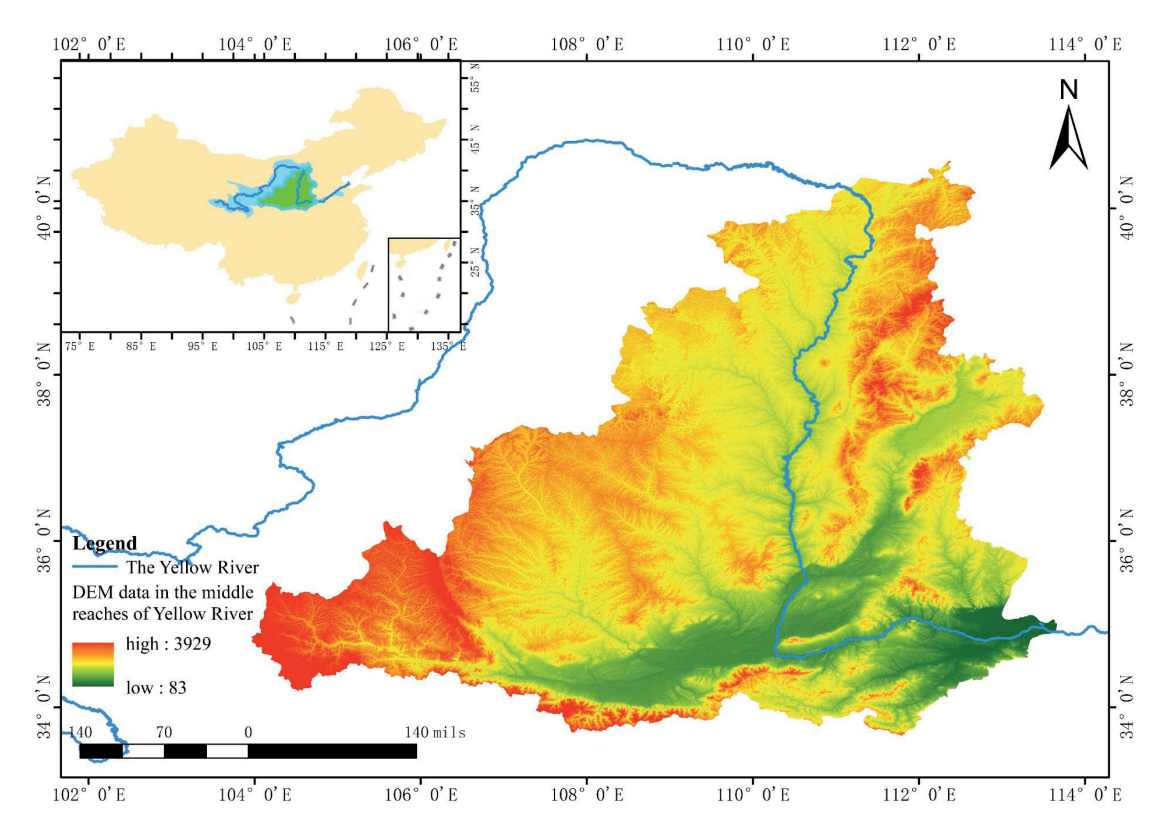


Fig. 1. Geospatial characteristics map of the Middle Reaches, Yellow River Basin.

Data Source

This study analyzed 67-year (1956-2022) annual precipitation records obtained from 15 surface meteorological stations (Dongsheng, Hohhot, Jiexiu, Linfen, Luochuan, Taiyuan, Yulin, Zhengzhou, Suide, Long, Sanmenxia, Huan, Kongtong, Wugong, and Min) and long-term mean annual precipitation data from 230 counties or districts across the middle reaches of the Yellow River Basin. The datasets were sourced from the China Meteorological Data Service Center (http://data.cma.cn/), national and provincial statistical yearbooks, and municipal government portals. Cubic spline interpolation, a widely used technique in meteorological data processing, was applied to ensure spatiotemporal consistency of the precipitation series to support robust analysis.

Methods

Mann-Kendall Trend Test and Abrupt Change Test

The Mann-Kendall test, recommended by the World Meteorological Organization (WMO) as a standard nonparametric statistical method [25], is widely employed to detect monotonic trends in time series data. For a time series $X = (x_1, x_2, ..., x_n)$, the test statistic S is calculated as:

$$S = \sum_{i=1}^{n-1} \sum_{j=i+1}^{n} sgn(x_j - x_i)$$
 (1)

where the $sgn(\cdot)$ function is defined by:

$$sgn(\theta) = \begin{cases} 1, & \theta > 0 \\ 0, & \theta = 0 \\ -1, & \theta < 0 \end{cases}$$
 (2)

For $n \ge 10$, S approximately follows a normal distribution with mean E(S) = 0 and variance:

$$Var(S) = \frac{n(n-1)(2n+5)}{18}$$
 (3)

The standardized test statistic Z is computed as:

$$Z = \begin{cases} \frac{S-1}{\sqrt{Var(S)}}, & S > 0\\ 0, & S = 0\\ \frac{S+1}{\sqrt{Var(S)}}, & S < 0 \end{cases}$$
(4)

Here, Z>0 indicates an increasing trend, Z<0 a decreasing trend. $|Z| \ge 1.96$ denotes significant at $\alpha = 0.05$. To quantify the trend magnitude, Sen's slope estimator (β) is applied:

$$\beta = Median\left(\frac{x_i - x_j}{i - j}\right) \quad 1 < j < i < n$$
 (5)

where β >0 indicates an upward trend and β <0 a downward trend, with absolute values reflecting the trend strength.

The Mann-Kendall abrupt change test method was utilized. For a given time series X, a rank-based sequential statistic S_k is constructed as:

$$S_k = \sum_{i=1}^k r_i, r_i = \begin{cases} 1, x_i < x_j \\ 0, x_i \le x_j \end{cases}$$
 (6)

with j = 1, 2, ..., i and k = 2, 3, ..., n. Under the assumption of independence, S_k has expectation and variance:

$$E(S_k) = \frac{n(n+1)}{4}, \quad 1 \ll k \ll n$$
 (7)

$$Var(S_k) = \frac{n(n-1)(2n+5)}{72}, 1 \ll k \ll n$$
 (8)

The standardized statistic *UF* is derived as:

$$UF = \frac{S_k - E(S_k)}{\sqrt{Var(S_k)}} \tag{9}$$

Reverse the time series, apply the same procedure to calculate UF, then take its negative value to obtain UB. Intersections between UF and UB curves within the critical bounds (± 1.96 at $\alpha = 0.05$) indicate significant change points. It should be noted that the Mann-Kendall abrupt change detection method performs significance testing on abrupt change points in time series trends.

Pettitt Test

Pettitt test is a non-parametric method based on the Mann-Whitney statistic [26]. Unlike the Mann-Kendall test, the Pettitt test specifically identifies mean change points in time series. The Mann-Whitney test statistic is calculated as:

$$U_{t,M} = U_{t-1,M} + \sum_{i=1}^{n} \operatorname{sgn}(x_t - x_j)$$

$$t = 2, 3, 4 \cdots, M$$
(10)

the following parameters are derived:

$$K_{t,M} = max \mid U_{t,M} \mid, (1 \leqslant t \leqslant M)$$
(11)

$$P = 2 \exp\left\{-\frac{6K_{t,M}^2}{M^3 + M^2}\right\} \tag{12}$$

here, t represents the temporal point in the series, $K_{t,M}$ is the test statistic, and P denotes the corresponding probability value.

Morlet Wavelet Analysis

This study employs the Morlet wavelet for periodicity analysis. Let the wavelet function be $\varphi(T) \in L^2(R)$.

The continuous wavelet transforms (CWT) for a function $f(t) \in L^2(R)$ is defined as:

$$W_{f(a, b)} = \langle f, \varphi_{a, b} \rangle = |a|^{-\frac{1}{2}} \int_{R} f(T) \overline{\varphi\left(\frac{T-b}{a}\right)} dT$$
(13)

where a is the scale factor, b is the translation factor, R is the set of all non-zero real numbers, $W_{f(a,b)}$ represents the wavelet coefficients. The mother function of the Morlet wavelet is expressed as:

$$\Psi(T) = exp\left(g\omega_0 T - \frac{T^2}{2}\right) \tag{14}$$

where $\Psi(T)$ is the basic wavelet function, ω_{θ} represents a fixed parameter (typically taken as 6 to satisfy the admissibility condition), and g is the imaginary unit, T denotes time.

Kruskal-Wallis H Test

For independent samples that satisfy the assumptions of normality and homogeneity of variance, parametric tests such as the T-test (for two groups) or one-way ANOVA (for multiple groups) are appropriate. When these assumptions are violated, nonparametric alternatives should be adopted. Considering the multigroup comparisons in this study, the Kruskal-Wallis H test was selected for hypothesis testing [27]. The test statistic is calculated as:

$$H = \frac{12}{N(N+1)} \left(\sum_{v=1}^{R_v^2} -3(N+1) \right)$$
 (15)

where H represents the test statistic, m_p denotes the sample size of the p-th group, N is the total sample size $(N = \Sigma m_p)$, and R_p is the sum of ranks for the p-th group. When ties are present in the data, a correction factor is applied to calculate the adjusted statistic H_c :

$$H_c = \frac{H}{C} \tag{16}$$

$$C = 1 - \frac{\sum (v_q^3 - v_q)}{N^3 - N} \tag{17}$$

Here, C represents the tie correction coefficient; v_q indicates the number of observations sharing the q-th tied rank (q = 2, 3, ..., m).

Moran's I

Moran's *I* is a widely used geostatistical method for quantifying the spatial dependence of geographical elements, comprising both global and local spatial autocorrelation analyses [28]. The global Moran's *I* evaluates whether spatial adjacency or proximity influences attribute values among regional units, thereby determining the presence of clustered or dispersed

patterns across the entire study area. The global Moran's *I* is calculated as:

$$I = \frac{\rho \sum_{h=1}^{\rho} \sum_{u=1}^{\rho} [W_{hu}(|x_h - \bar{x}||x_u - \bar{x}|)]}{\sum_{h=1}^{\rho} \sum_{u=1}^{\rho} [W_{hu}(|x_u - \bar{x}|^2)]}$$
(18)

$$Z = \frac{I - E(I)}{\sqrt{VAR(I)}} \tag{19}$$

Here, h and u represent different regions, respectively; ρ is the num of regions; I represents the global Moran's I (ranging from -1 to 1); ρ denotes the number of sampled cities; W_{hu} constitutes a binary spatial weight matrix (1 for adjacent cities h and u, 0 otherwise); and \bar{x} is the mean attribute value.

Local spatial autocorrelation analysis serves to quantify the similarity between a given spatial unit and its neighboring units with respect to specific attribute values. This method is particularly valuable for identifying spatial clusters (hot spots or cold spots) and detecting spatial heterogeneity in hydrological and environmental datasets. The local Moran's I_h is computed as follows:

$$I_{h} = \frac{(x_{h} - \bar{x}) \sum_{u=1}^{\rho} [W_{hu}(x_{u} - \bar{x})]}{S^{2}}$$
(20)

where S^2 represents the variance of variable x; $I_h > 0$ indicates positive spatial autocorrelation (clustering of similar values); $I_h < 0$ suggests negative spatial autocorrelation (dispersion of similar values); $I_h = 0$ implies random spatial distribution.

Results and Discussion

Spatio-Temporal Trend Characteristics Analysis in the Middle Reaches of the Yellow River Basin

Trend Detection Analysis

A Mann-Kendall trend analysis was conducted on the 67-year (1956-2022) annual precipitation series from the 15 monitoring stations, and the results are summarized in Table 1.

The Mann-Kendall test results ($\alpha = 0.05$) indicated no statistically significant trends in precipitation at any of the 15 monitoring stations (|Z|<1.96). However, spatially heterogeneous patterns were observed. The northern region exhibited increasing trends (Z>0), with Yulin showing the most pronounced increase ($\beta = 1.05 \text{ mm yr}^{-1}$). Southeastern sectors displayed decreasing trends (Z<0), with Jiexiu experiencing the most rapid declines $(\beta = -0.90 \text{ mm yr}^{-1})$. Sanmenxia $(\beta = -0.65 \text{ mm yr}^{-1})$ and Zhengzhou ($\beta = -0.63$ mm yr¹) demonstrated intermediate decline rates. The southwestern region exhibited divergent trends, such as Kongtong $(\beta = 0.37 \text{ mm yr}^1)$, Wugong $(\beta = -0.56 \text{ mm yr}^1)$,

and Long (β = -0.92 mm yr¹), showing varying magnitudes of change. This spatial heterogeneity suggests that precipitation dynamics in this area may be influenced by complex local factors. Other stations exhibited minimal trends ($|\beta|$ <0.5 mm yr¹). Collectively, suggest that precipitation patterns have remained generally stable over the past few decades.

The spatial distribution pattern of precipitation trends was generated using inverse distance weighting (IDW) interpolation of the Sen's slope coefficients (β), as shown in Fig. 2.

The northwestern regions exhibited an overall increasing trend in precipitation, while the southeastern areas showed a decreasing trend, with more pronounced declines observed in proximity to the lower basin of

this area. Notably, localized anomalies were detected, such as increasing precipitation trends at Min and Long stations in the southeastern sector. However, Mann-Kendall test results (Table 1) indicated that neither the increasing nor the decreasing trends were statistically significant ($\alpha=0.05$). These findings are consistent with Liu et al., who reported a non-significant declining trend (1960-2020) at the Yinchuan meteorological station, suggesting regionally coherent sub-significant precipitation variability [29].

Mann-Kendall trend analysis revealed spatially heterogeneous precipitation patterns across the 15 monitoring stations. Eight stations (Yulin, Kongtong, Min, Taiyuan, Dongsheng, Hohhot, Huan, and Suide) exhibited increasing trends in annual precipitation,

Table 1. Results of Mann-Kendall trend analyst	sis for 15 stations.
--	----------------------

North	Dongsheng	Hohhot	Yulin	Suide	Taiyuan	
Z	0.12	0.11	1.32	0.01	0.18	
β (mm yr ⁻¹)	0.10	0.13	1.05	0.003	0.18	
Southeast	Jiexiu	Luochuan	Linfen	Sanmenxia	Zhengzhou	
Z	-1.20	-0.06	-0.42	-0.61	-0.52	
β (mm yr ¹)	-0.9	-0.07	-0.34	-0.65	-0.63	
Southwest	Huan	Wugong	Kongtong	Long	Min	
Z	0.06	-0.50	0.44	-0.87	0.23	
β (mm yr ⁻¹)	0.04	-0.56	0.37	-0.92	0.13	

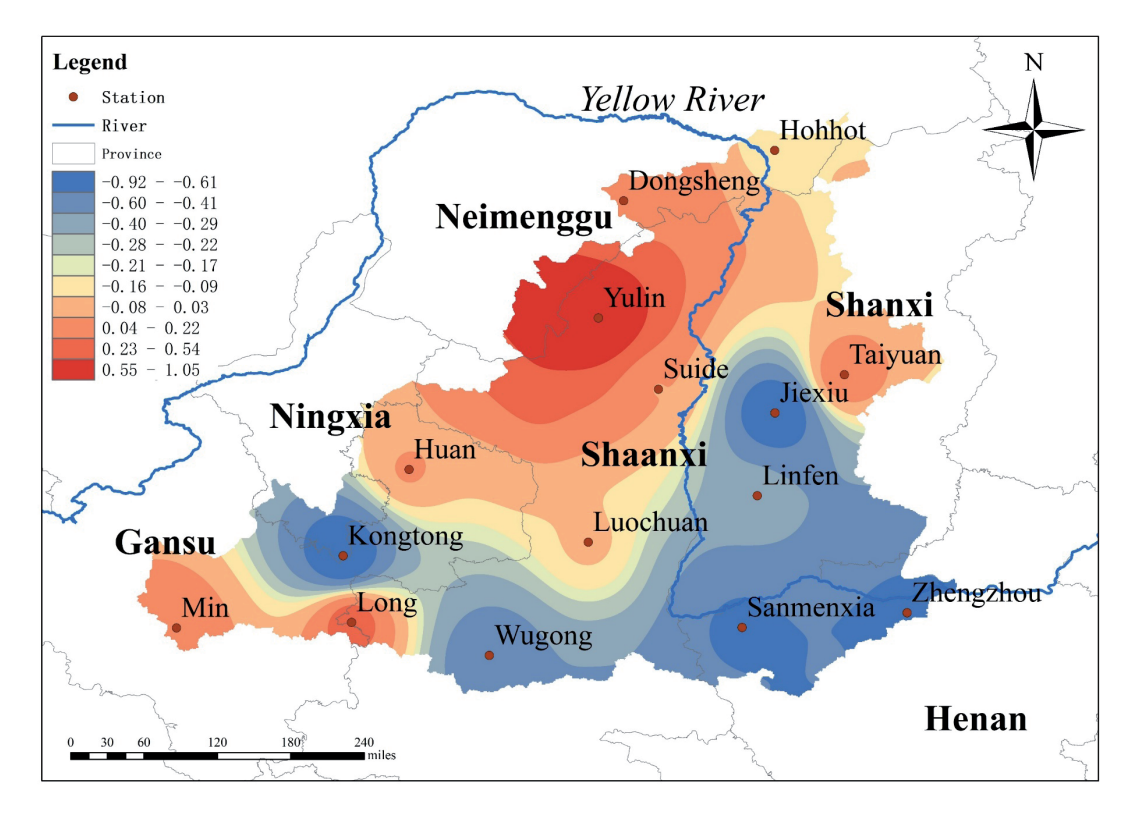


Fig. 2. Spatial interpolation map of Sen's slope values (β) in the middle reaches of the Yellow River Basin.

although none were statistically significant at $\alpha = 0.05$. Conversely, 7 stations (Jiexiu, Long, Sanmenxia, Wugong, Zhengzhou, Linfen, and Luochuan) showed decreasing trends, which were also statistically non-significant, with only marginal variations observed.

Owing to the long time series adopted in this study, small-scale regions may lack a consistent variation trend over the entire period. Nevertheless, some discernible changes can still be identified within certain short-term intervals. For instance, while Wugong station displayed no significant trend over the entire period, a statistically significant decline was detected during the sub-period 1993-2006. Spatially, the middle Yellow River Basin demonstrated a distinct precipitation pattern: marginal increases in the northeastern and southwestern sectors contrasted with slight decreases in the southern and southwestern regions. This spatial gradient likely reflects the complex interplay between regional atmospheric circulation patterns and local topographic effects, which may modulate precipitation dynamics in the study area.

Change-Point Analysis

Variations in precipitation time series may manifest as either trend shifts or mean shifts. In this study, trend change points were detected using the Mann-Kendall abrupt change test, while mean change points were identified through Pettitt's test method. Fig. 3 shows the Mann-Kendall abrupt change test results.

The Mann-Kendall abrupt change detection identified several apparent transition points across northern stations, with Dongsheng exhibiting a change in 1978 (Fig. 3a)), Yulin in 2013 (Fig. 3c)), Hohhot in 1962 and 2022 (Fig. 3b)), and Taiyuan in 1965, 1968, and 2018 (Fig. 3f)). Notably, both Hohhot and Taiyuan showed changes in recent years, while Suide displayed no statistically significant transitions. Dense curve intersections were observed during short periods: 1956-1966 and 2012-2022 for Dongsheng (Fig. 3a)), 1978-2002 for Hohhot (Fig. 3b)). The temporal distribution of these potential change points demonstrated clear regional asynchrony.

Southeastern stations exhibited the following changes: Jiexiu exhibited changes in 1957, 1986, 1989, and 2020 (Fig. 3e)); Linfen in 2020 (Fig. 3g)); Luochuan in 1978 and 2018 (Fig. 3j)); Zhengzhou in 1960, 2003, and 2020 (Fig. 3i)); and Sanmenxia in 1970, 1978, 1990, 2009, 2015, and 2020 (Fig. 3h)). Linfen, Zhengzhou, and Luochuan showed consecutive intersection points in their detection curves. However, none of these transitions reached statistical significance.

In the southwestern region, significant change points were detected at: Huan (2011, 2013, and 2020) (Fig. 3n)), Kongtong at 2016 (Fig. 3o)), and Min (1958, 2017, and 2020) (Fig. 3m)). The test statistics for Min exhibited particularly wide variability throughout the study period, reflecting greater amplitude in precipitation variations that consequently resulted in more frequent detection of potential regime shifts. These findings

collectively highlight the spatial heterogeneity in precipitation variability across the study area, while emphasizing the importance of rigorous statistical validation in distinguishing genuine climatic transitions from natural variability.

Fig. 3 reveals that certain monitoring stations exhibit remarkably similar abrupt change points in their precipitation records. Notably, 5 geographically distant stations: Dongsheng (Fig. 3a)), Sanmenxia (Fig. 3h)), Luochuan (Fig. 3j)), Long (Fig. 3k)), and Min (Fig. 3m)) all experienced abrupt changes in 1978, suggesting the potential influence of large-scale climatic factors. Similarly, Zhengzhou (Fig. 3i)) and Suide (Fig. 3d)) underwent abrupt transitions in 2003. A particularly significant cluster of abrupt changes occurred in 2020, affecting 6 southern stations in the middle Yellow River region: Sanmenxia (Fig. 3h)), Zhengzhou (Fig. 3i)), Linfen (Fig. 3g)), Long (Fig. 3k)), Min (Fig. 3m)), and Huan (Fig. 3n)), indicating pronounced hydrological variations across the southern sector. During this period, precipitation exhibited exceptional intensity, with Long receiving 900 mm and Min exceeding 1000 mm of annual rainfall. These extreme precipitation events directly contributed to severe flooding in downstream areas of Henan and Anhui provinces, including the Second 2020 Yellow River Flood (August 21st at Tongguan hydrological station) and the August 17th Wei River Flood. Liu et al previously identified that abrupt hydrological modifications in the middle Yellow River predominantly occur south of 38°N latitude [30], with most transitions concentrated between 1963-1998 prior to 2006, a finding consistent with our observations at Luochuan (Fig. 3j)), Sanmenxia (Fig. 3h)), and Min (Fig. 3m)) stations.

Furthermore, precipitation regime shifts may be influenced by multiple factors. Chang et al. analyzed precipitation and runoff data from 68 gauging stations across the Yellow River Basin, revealing that abrupt change points were primarily clustered between the midstream (Huayuankou) and downstream (Lijin) sections [31]. Notably, the key transition years (1990 and 2010) aligned with abrupt shifts observed at Jiexiu and Zhengzhou stations in this study. Furthermore, precipitation regime shifts may be confounded by other drivers. Wang et al. analyzed the spatiotemporal evolution and driving forces of drought characteristics in the Yellow River Basin [32], revealing significant precipitation variations around 2000 that align with our findings of marked hydrological changes during this period. These synchronous transitions suggest precipitation dynamics may be affected by additional external forcings, potentially including vegetation changes, runoff modifications, and intensified industrial activities due to human exploitation in the region, which could collectively contribute to the observed precipitation fluctuations. A comprehensive analysis of precipitation variations in the middle Yellow River region from 1956 to 2022 reveals distinct abrupt changes occurring predominantly in 1978, 2003,

and 2020, with an observable intensification of precipitation fluctuations in recent years. The southwestern sector exhibits significantly more frequent precipitation regime shifts compared to other subregions.

The increasing occurrence of abrupt change points, when considered alongside alterations in runoff patterns and precipitation trends, suggests a paradoxical hydrological scenario: while the total precipitation

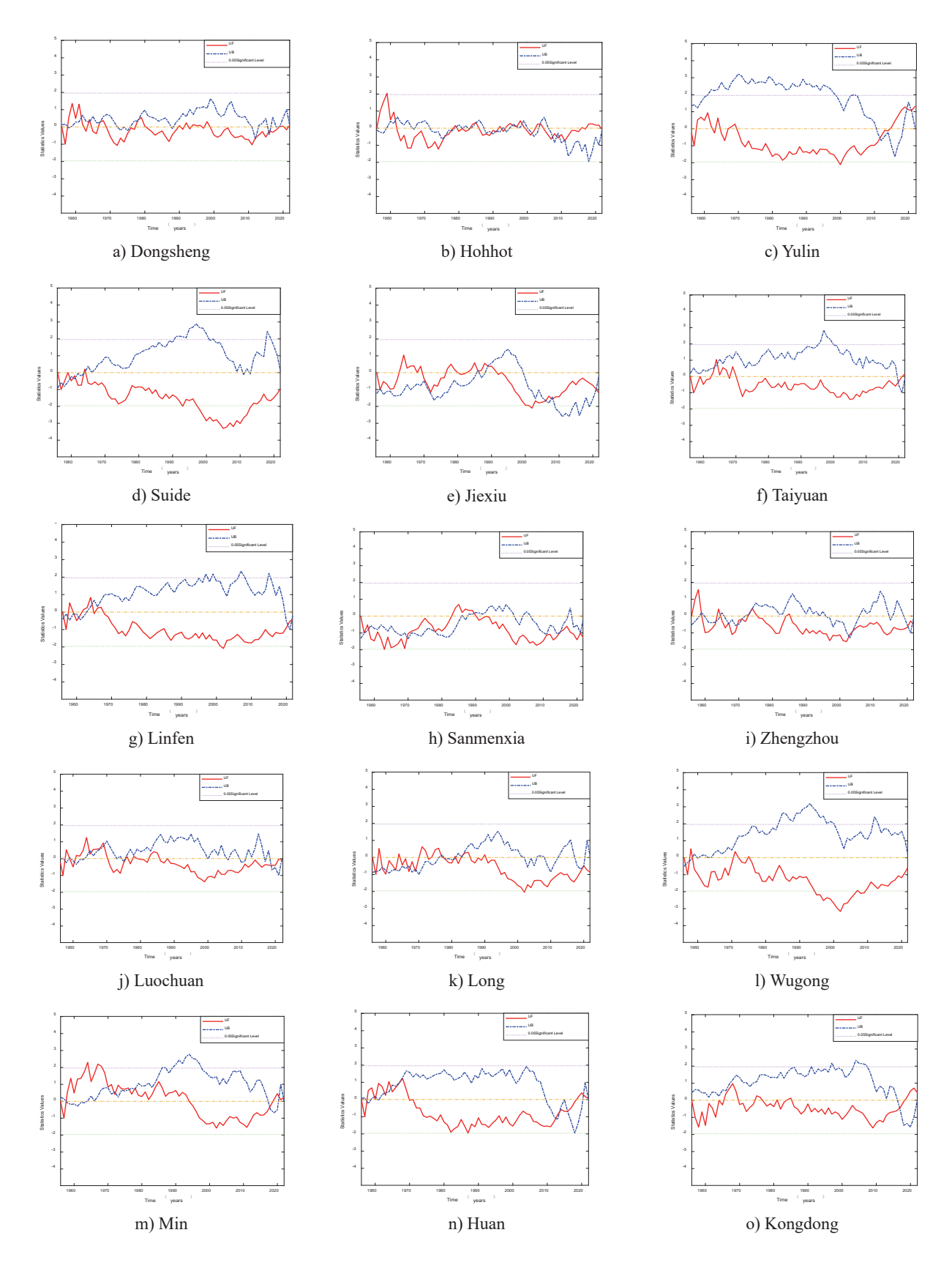


Fig. 3. The spatiotemporal distribution of precipitation abrupt change points at 15 stations.

North	Dongsheng	Hohhot	Yulin	Suide	Taiyuan	
loc	6	6	60	30	14	
K	87	127	256	307	164	
P(loc)	1.7235	1.4566	0.5516	0.3137	1.1788	
Southeast	Jiexiu	Luochuan	Linfen	Sanmenxia	Zhengzhou	
loc	39	14	21	39	30	
K	300	148	230	276	199	
P(loc)	0.341	1.3003	0.7071	0.4475	0.9183	
Southwest	Huan	Wugong	Kongtong	Long	Min	
loc	13	29	13	35	30	
K	210	304	114 246		109	
	İ	İ	İ		1	

1.5491

0.3252

Table 2. Results of the Pettitt test for 15 stations.

P(loc)

frequency has increased with enhanced temporal continuity, the reduction in moderate rainfall events has exacerbated water resource scarcity [33]. This precipitation regime transformation presents a critical challenge for water resources management in the basin, where more frequent precipitation is paradoxically coupled with heightened water stress due to the declining contribution of moderate rainfall events to water recharge.

0.8406

Subsequent Pettitt's tests yielded all p-values>0.05 (Table 2), indicating no statistically significant mean shift positions at these 15 stations in the middle Yellow River region. This finding emphasizes the necessity of applying complementary change-point detection methods in hydroclimatic studies to distinguish between authentic hydrological transitions and stochastic variations in precipitation patterns. In summary, the precipitation in the middle Yellow River region exhibits statistically significant abrupt changes in trends at certain locations, while no significant shifts in mean values are observed. This suggests that regional precipitation is influenced by external factors, such as climatic variations or anthropogenic activities, whose intensities or directional effects may have fluctuated over time. However, these influences collectively have not substantially altered the long-term mean annual precipitation pattern across the study area.

Periodic Characteristics

The periodic characteristics of annual precipitation series from 15 stations were examined using the Morlet wavelet analysis, yielding the real-part coefficient diagram (Fig. 4) and wavelet variance diagram (Fig. 5).

The northern stations exhibit three distinct periodic characteristics at 5-10, 15-25, and 30-50a timescales. As evidenced by the absolute energy values in Fig. 4, these periodic components generally intensify over time,

though Taiyuan demonstrates relatively weaker energy at the 30-50a scale (Fig. 4f)). Notably, some periodic features appear phase-dependent: Hohhot displays a 15-25a periodicity emerging around 1990 (Fig. 4b)), while Suide shows pronounced 15-25a oscillations before 2000 that gradually diminish thereafter (Fig. 4d)). The precipitation variability across northern stations demonstrates marked differences in energy distribution and periodicity across temporal scales, with evident phase-dependent characteristics.

0.6087

1.5835

In contrast, the southeastern stations display more complex periodic structures. Jiexiu (Fig. 4e)) and Luochuan (Fig. 4j)) exhibit significant cycles at 5-10, 15-25, 35-45, and 50-60a scales, while Linfen (Fig. 4g)) and Sanmenxia (Fig. 4h)) demonstrate dominant periodicities at 5-10, 20-30, and 30-45a intervals. Zhengzhou (Fig. 4i)) presents a unique temporal pattern, with 5-15a cycles predominating before 1990 that subsequently bifurcate into distinct 5-10a and stronger 20-45a periodic components post-1990. Overall, the southeastern stations exhibit more robust energy signatures and clearer periodic features compared to their northern counterparts, suggesting greater temporal organization in precipitation variability within this subregion. This spatial differentiation in precipitation periodicity may reflect underlying differences in climatic controls or geographical influences across this area. The 5 southwestern stations share common cycles at 5-10, 20-30, and 40-55a scales, with energy intensity following 40-55a (strongest) >5-10a>20-30a (weakest). Min exhibits notably lower energy until 2010, when its periodicity becomes more pronounced.

Station-specific analysis shows Linfen's simpler dual-period structure suggests fewer dominant controls (Fig. 5b)), while Dongsheng (Fig. 5a)), Jiexiu (Fig. 5b)), Yulin (Fig. 5a)), Zhengzhou (Fig. 5b)), and Wugong (Fig. 5c)) stations with four primary cycles indicate more complex precipitation drivers. The wavelet variance

spectrum (Fig. 5) identifies primary cycles through peak values, where the maximum peak corresponds to the dominant period (longest oscillation scale), followed by secondary and tertiary cycles. This multi-scale analysis provides critical insights into the temporal organization of precipitation variability across the study area, highlighting significant regional differences

in periodicity characteristics and potential driving mechanisms.

Wavelet variance analysis of northern stations (Fig. 5a)) reveals distinct yet partially coherent periodic characteristics. Taiyuan station exhibits three dominant periodic peaks at 43, 24, and 5a, while Yulin station demonstrates four peaks at 44, 18, 12, and 8a, and Suide

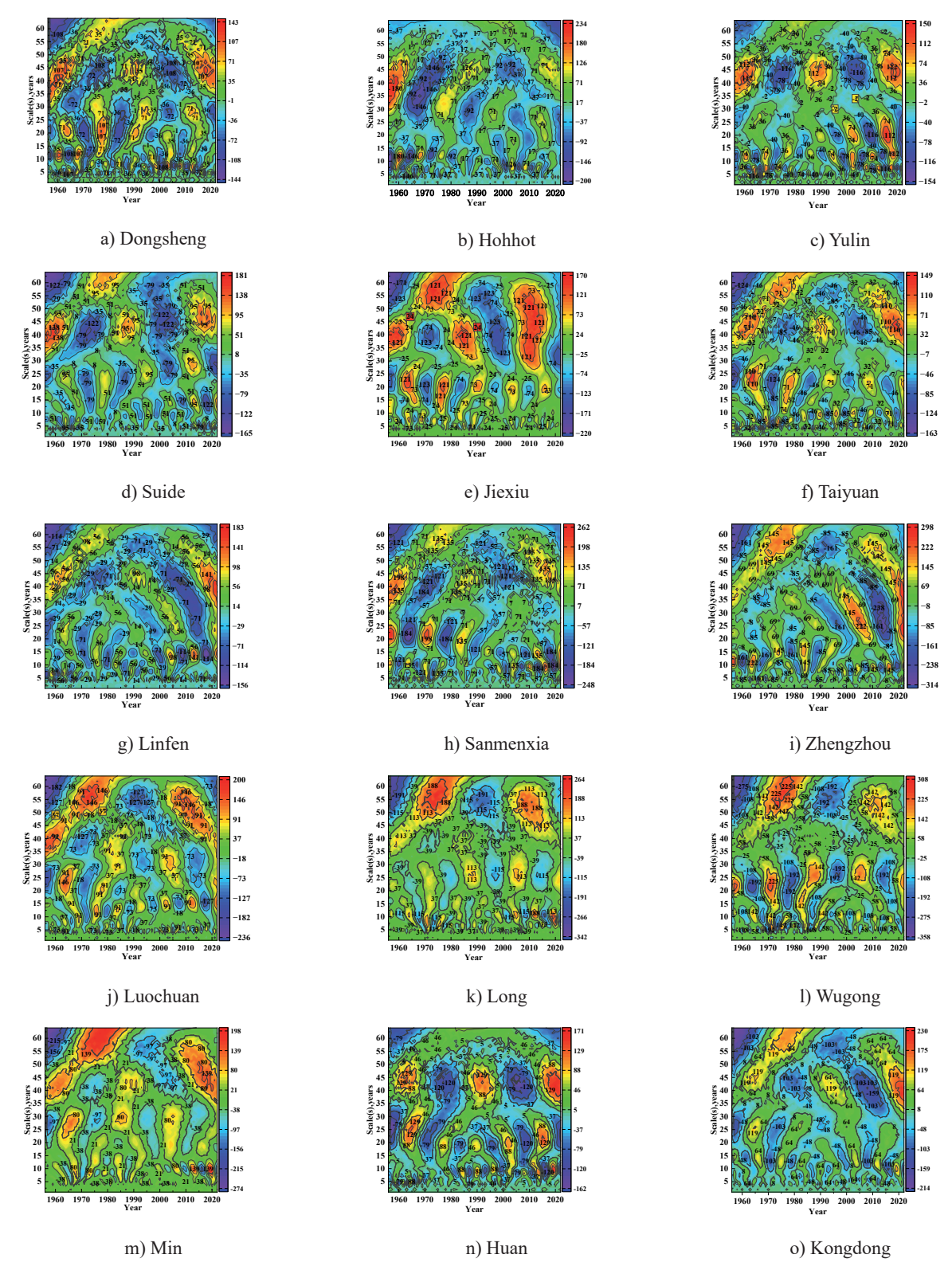


Fig. 4. Real part diagram of wavelet analysis coefficients for 15 stations.

station shows three peaks at 44, 28, and 14a. Notably, these 3 stations share similar primary periodicities in their first dominant cycles. Hohhot station displays three significant periods at 37, 12, and 8a, whereas Dongsheng station presents four distinct periods at 45, 20, 12, and 5a intervals, with these 2 stations maintaining identical secondary and tertiary periodic components. Despite spatial variability induced by multiple influencing factors, the northern stations retain partially shared or similar dominant periodic patterns in their precipitation characteristics.

As shown in Fig. 5b), the southeastern stations exhibit distinct periodic characteristics: Linfen displays two dominant peaks at 43 and 14a cycles, while Sanmenxia shows three peaks at 44, 22, and 10a intervals, with both stations sharing similar primary periodicities. Jiexiu demonstrates four significant cycles at 56, 42, 30, and 14a scales, Zhengzhou exhibits 56, 35, 22, and 10a cycles, and Luochuan presents 56, 25, and 15a periods. These 3 stations share identical primary periodicities with longer timescales compared to other stations in both northern and southeastern stations, while their secondary cycles closely match the primary

periods of other southeastern stations and most northern sites. In the southwestern stations (Fig. 5c)), Min station shows peaks at 44, 29, and 10a cycles, Huan at 44, 20, and 10a intervals, and Kongtong at 44, 26, and 10a scales, all sharing similar primary periodicities. Long exhibits three peaks at 55, 26, and 10a cycles, while Wugong county displays four distinct periods at 56, 25, 10, and 5a intervals.

Notably, multiple stations demonstrate identical or similar dominant cycles: Jiexiu, Luochuan, Zhengzhou, Wugong, and Long share approximately 56a primary cycles; Taiyuan, Yulin, Suide, Sanmenxia, Huan, Kongtong, and Min exhibit around 44a primary periods; and Hohhot, Yulin, Zhengzhou, Sanmenxia, Huan, Kongtong, Long, Wugong, and Min all possess approximately 10a dominant cycles, suggesting coherent precipitation patterns across the study region despite geographical variations.

The precipitation regime in the middle reaches of the Yellow River Basin is characterized by three predominant periodic variations at 5-10, 15-30, and 30-55a timescales. Regional analyses reveal significant spatiotemporal heterogeneity in these periodic

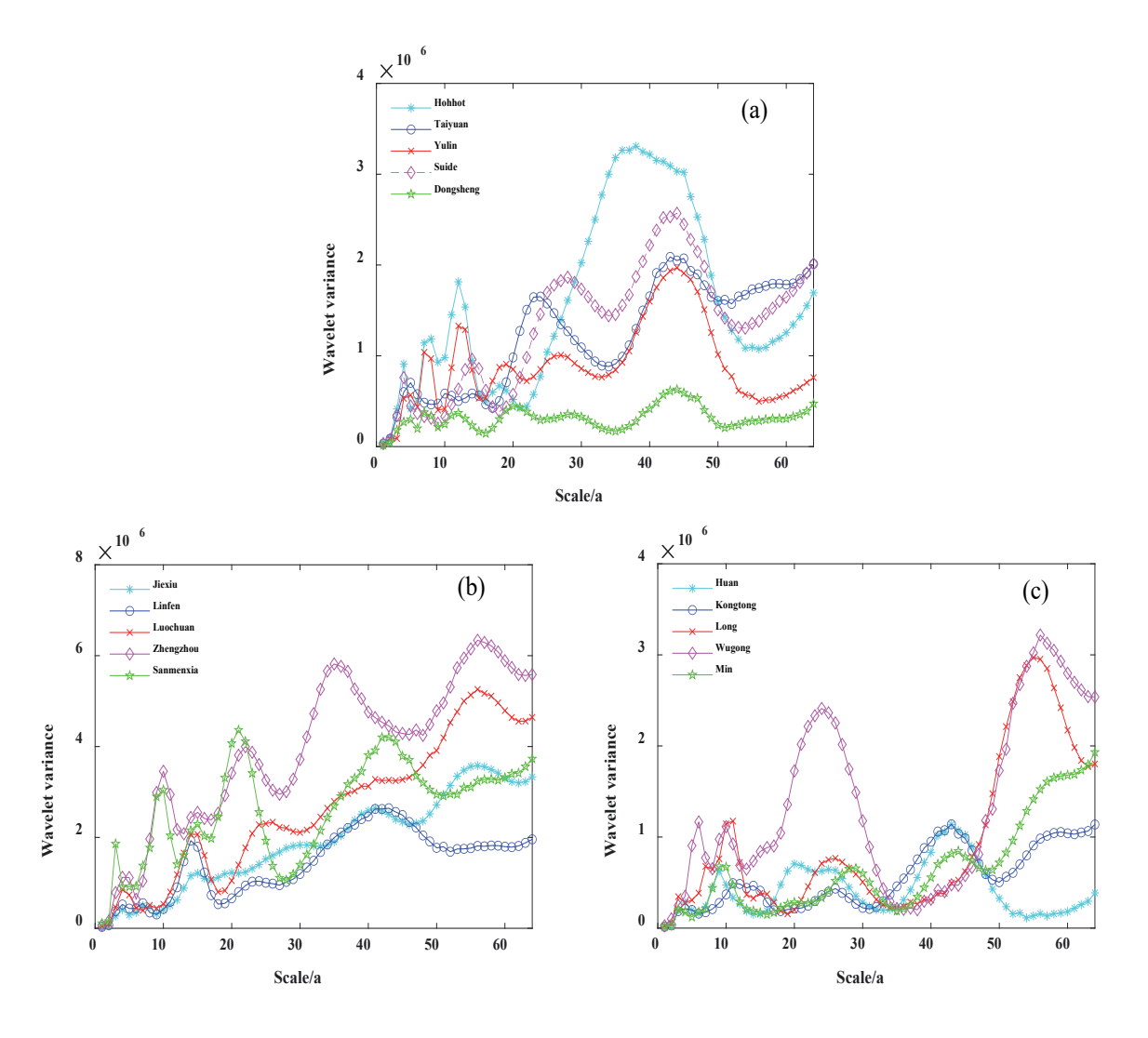


Fig. 5. Variance diagram of Wavelet Analysis. a) Northern, b) Southeastern, c) Southwestern.

patterns, with particularly pronounced temporal-scale amplifications and attenuations observed in the timedependent periodicity variations. The year 1990 appears to represent a critical transition point for precipitation pattern shifts in the region, as evidenced by substantial alterations in periodic characteristics at several monitoring stations, notably Yulin (Fig. 4c)), Jiexiu (Fig. 4e)), and Zhengzhou (Fig. 4i)). Basin-scale examination identifies three primary cycles of approximately 10, 44, and 56a as the dominant periodic components governing precipitation variability across the middle Yellow River region, suggesting the coexistence of both localized climatic influences and large-scale atmospheric controls operating at these characteristic temporal scales.

Analysis of the Spatial Characteristics of Precipitation

Spatial Heterogeneity of Annual Precipitation Regimes Across 15 Stations

Initial normality testing was performed on each dataset (N=67>50) using the Kolmogorov-Smirnov (K-S) test as the primary method, with the Shapiro-Wilk (S-W) test serving as supplementary reference [34]. The analytical results revealed non-normal distributions in precipitation data from the Sanmenxia, Wugong, and Zhengzhou stations (all p-values<0.05). Subsequent Levene's test for homogeneity of variances yielded statistically significant results (p<0.05). These collective findings precluded the application of parametric analysis of variance (ANOVA). Given the presence of multiple

independent sample groups (≥3) in this study, the nonparametric Kruskal-Wallis H test was subsequently adopted for comparative analysis of precipitation differences [35], with detailed results presented in Table 3.

The results demonstrated that the annual precipitation series of Hohhot and the Dongsheng show no significant differences at the northern stations (e.g., Jiexiu, Taiyuan, and Yulin), whereas significant disparities were observed at the remaining stations compared to the Dongsheng, which may be attributed to latitudinal influences. Similarly, the Min station in the south exhibits no significant differences in annual precipitation only with regions at similar latitudes, whereas pronounced variations are found in geographically distant areas. Comparable patterns are observed in Zhengzhou, Luochuan, Sanmenxia, and other regions. Thus, latitudinal-induced climatic variations remain a critical factor influencing precipitation distribution.

The violin plots of precipitation for the 15 stations are presented in Fig. 6, which reveals that the southeastern part of the middle Yellow River region, including Luochuan, Zhengzhou, Sanmenxia, and Wugong, exhibits generally higher rainfall amounts, indicating both elevated precipitation levels and spatial concentration. In contrast, lower precipitation is observed in northern stations such as Hohhot, Taiyuan, Yulin, and Dongsheng. From west to east, precipitation demonstrates an increasing trend, and the 400 mm isohyet in the Yellow River Basin aligns closely with the boundary between China's semi-humid and semi-arid regions, suggesting a spatial pattern of decreasing precipitation from the southeast to the northwest in

Table 3. Kruskal-Wallis H Test results across 15 stations.

	ZZ	LC	WG	M	L	SMX	KT	LF	SD	JX	TY	Н	YL	Hohhot
DS	0*	0*	0*	0*	0*	0*	0*	0.014*	0.62	1	1	1	1	1
Hohhot	0*	0*	0*	0*	0*	0*	0.002*	0.273	1	1	1	1	1	
YL	0*	0*	0*	0*	0*	0*	0.007*	0.713	1	1	1	1		
Н	0*	0*	0*	0*	0*	0*	0.139	1	1	1	1			
TY	0*	0*	0*	0*	0*	0.002*	0.554	1	1	1				
JX	0*	0*	0*	0*	0*	0.008*	1	1	1					
SD	0*	0*	0*	0*	0*	0.015*	1	1						
LF	0*	0*	0*	0.003*	0.008*	0.672	1							
KT	0.001*	0.031*	0.036*	0.434*	0.828	1								
SMX	0.345	1	1	1	1									
L	1	1	1	1										
M	1	1	1											
WG	1	1												
LC	1													

^{(*} indicates the rejection of the null hypothesis, $\alpha = 0.05$).

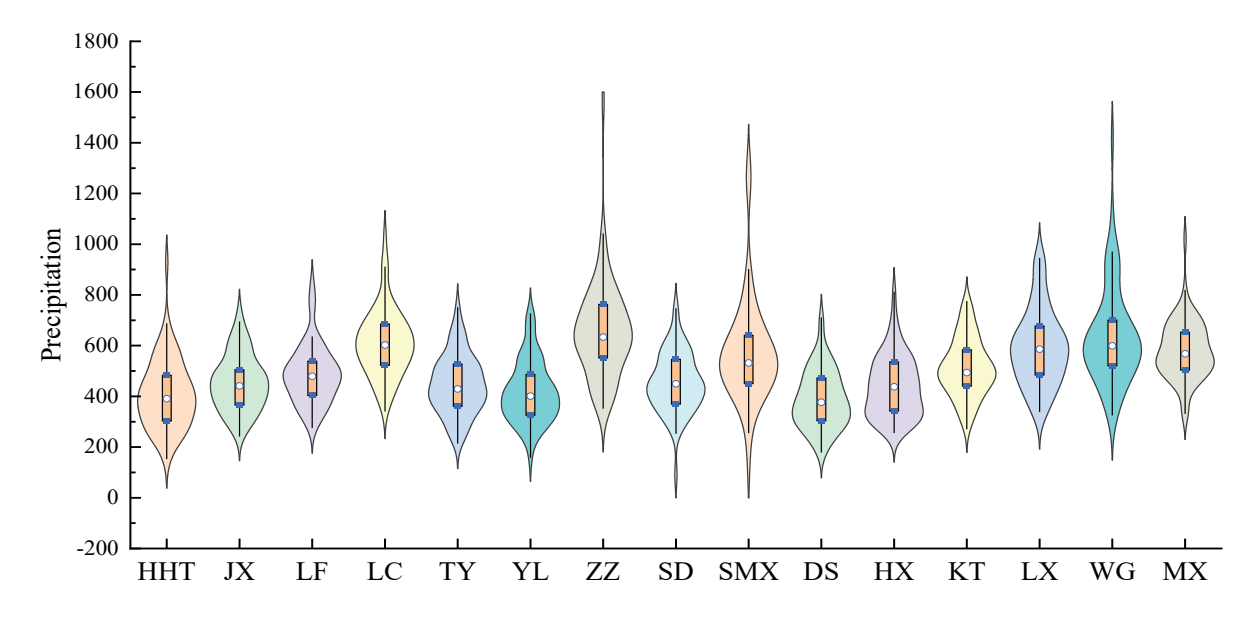


Fig. 6. Violin plot of precipitation at 15 stations. Note: In the violin plot, cerulean markers represent the 25th and 75th percentiles of precipitation, while the alabaster central circle marks the median (50th percentile). The width of the violin reflects data density via kernel density estimation, with wider areas indicating higher probability density.

the middle Yellow River region [36]. The interannual variability in precipitation across this area is closely linked to regional differences. Previous studies on the entire Yellow River Basin have identified a longitudinal zonation characteristic with no clear latitudinal linear relationship, which contrasts with the findings of this study. This discrepancy may arise because the present research focuses specifically on the middle Yellow River region, where the longitudinal span is relatively small, while the latitudinal gradient is sufficiently pronounced [37].

The results in Table 2 indicate that no significant differences in annual precipitation exist among geographically proximate regions, whereas pronounced disparities are observed in areas with substantial spatial separation. This pattern aligns well with the documented characteristics of precipitation variability, which exhibits a wide range of fluctuations [38]. Furthermore, precipitation in China is predominantly concentrated in the summer months, with higher amounts in the south and lower amounts in the north, a finding that further corroborates the observed north-south precipitation gradient in the middle Yellow River region [39].

Analysis of the Spatial Autocorrelation of Precipitation

This study employs both global and local Moran's I indices to conduct an in-depth spatial autocorrelation analysis of multi-year average annual precipitation across 230 counties/districts in the middle reaches of the Yellow River. The results demonstrate a statistically significant positive spatial correlation, with a global Moran's I of 0.5533 ($Z=18.2730,\ p<0.05$), indicating pronounced

spatial clustering of precipitation patterns among these counties. Further local spatial autocorrelation analysis, as illustrated in Fig. 7, reveals distinct spatial aggregation characteristics of precipitation distribution across the study area.

Fig. 7 reveals distinct spatial clustering patterns of multi-year average precipitation across the middle Yellow River region. The red areas represent high-high (HH) clusters, indicating regions with consistently high precipitation concentrated mainly in the southern sector. Conversely, blue zones denote low-low (LL) clusters with persistently low precipitation, predominantly located in the northern areas. Green areas exhibit low-high (LH) anomalies where localized dry zones are surrounded by wetter regions. Notably, no high-low (HL) clusters (wet centers surrounded by dry areas) were observed in this study area.

An interesting anomaly occurs in the southwestern portion, where several southern counties exhibit LL clustering characteristics despite their lower latitude position. This phenomenon is attributed to their location within Gansu Province's arid climate zone, where precipitation patterns are dominated by the East Asian monsoon - yielding abundant summer rainfall but winter drought conditions due to westerly winds and cold air masses [40]. The LH anomalies observed in southern areas, particularly in Xincheng District (Xi'an) and Qindu District (Xianyang), likely result from urbanization-induced hydrological imbalance combined with orographic effects of the Qinling Mountains [41], where windward slopes receive enhanced rainfall while leeward areas experience rain shadows. Over recent decades, significant land use changes - marked by increased construction land and decreased forest,

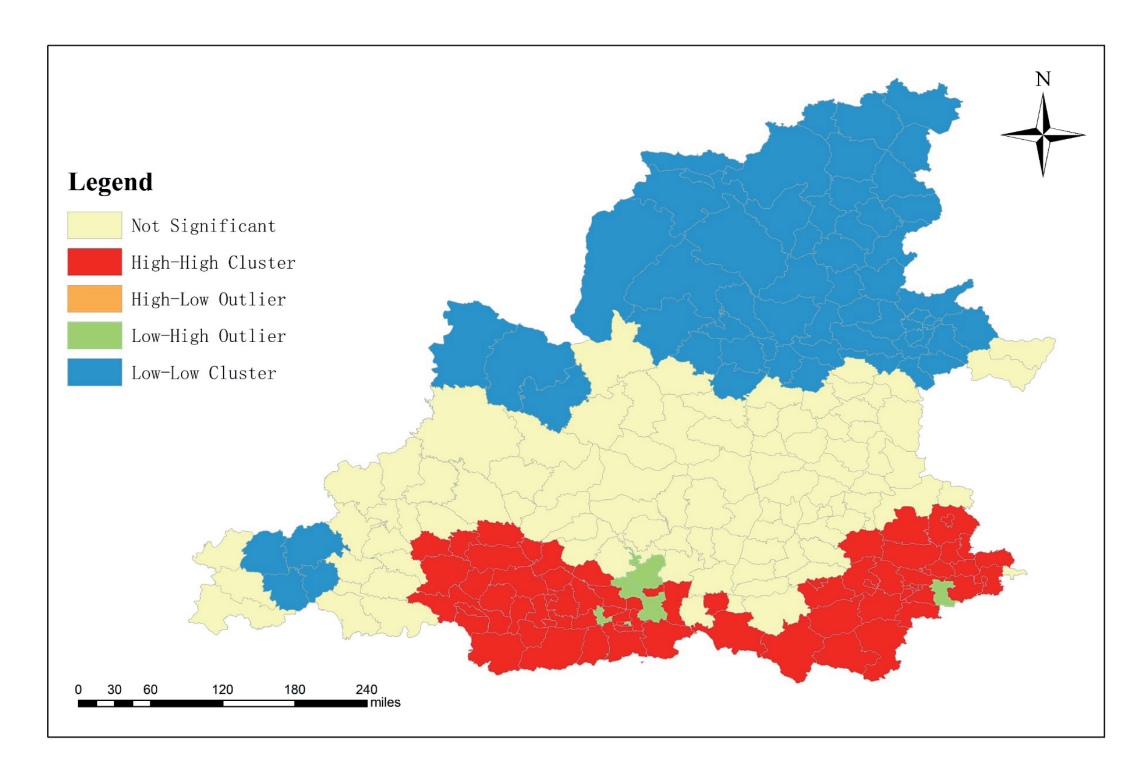


Fig. 7. Analysis diagram of local Moran's I.

grassland, and water areas - have substantially modified local climate conditions and precipitation patterns throughout the Yellow River Basin [42].

Precipitation, Regional Hydrological Cycle, and Vegetation Change Processes

Analysis of multi-decadal hydrological records from the Yellow River Basin reveals a declining trend in both streamflow and precipitation, with the streamflow reduction being more pronounced [43, 44]. However, this study finds no statistically significant trend in precipitation, suggesting that the observed streamflow reduction during recent decades has been primarily driven by non-precipitation factors.

The rapid industrial development and continuously increasing water consumption, coupled with expanded human activities due to improved living standards, have significantly exacerbated water stress in the Yellow River Basin [45]. Hydrological diagnostics revealed that precipitation variation constituted the dominant driver (contribution rate: 39.31%-54.70%) of runoff alterations in the upper Yellow River Basin during 1960-2020, while anthropogenic activities emerged as the principal forcing mechanism (contribution rate: 63.70%-84.37%) for runoff modifications in the middlelower reaches [46]. In addition, Zhao et al., through systematic analysis of streamflow and sediment flux series from 32 mainstream hydrological stations and 34 major tributary monitoring nodes in the Yellow River Basin (1960-2023) [47], identified dominant drivers and quantified their contribution rates, demonstrating that anthropogenic interventions constituted

primary contributors (87.77% and 84.16%) to runoff depletion and sediment yield reduction, while climatic factors contributed minimally (12.23% and 15.84%, respectively). These findings conclusively identify human activities as the dominant driver of streamflow variations in the Yellow River Basin during recent decades.

During the period 1990-2000, the Yellow River Basin experienced significant land use changes, with cultivated land, construction land, and unused land areas increasing by 2917 km², while grassland and woodland areas decreased by 4668 km² and 33 km², respectively [48]. Following the implementation of the Grain for Green Program, substantial vegetation restoration has been achieved across most regions. Analysis of NDVI trends between 2000 and 2010 revealed that 62.9% of vegetated areas showed improvement while 27.7% experienced degradation, with the remaining areas showing indeterminate changes [49]. From 2000 to 2022, the average annual vegetation coverage across the Loess Plateau increased by 0.86%, rising from 0.439 to 0.636 and transitioning from moderate to moderately high coverage levels [50]. A case study in the Jiuyuangou watershed of Suide, Shaanxi Province, demonstrated particularly striking results, with forest and grassland coverage increasing from 33.4% in 1995 to 74.1% by 2020 [51]. However, Feng et al. cautioned that vegetation restoration in the Loess Plateau region is approaching the sustainable water resource limit [52]. Chen et al. further noted that vegetation coverage has reached approximately 65% by 2021 after seven decades of continuous increase, approaching the upper threshold of ecological security [53]. Importantly, this large-scale vegetation recovery

has become a major contributing factor to reduced river runoff in the Yellow River, particularly under conditions of stable precipitation patterns.

A comprehensive investigation reveals a significant declining trend in annual sediment load of the Yellow River from 1950 to 2006, particularly in the lower reaches, where sediment discharge exhibited a pronounced reduction [54]. At the Lijin hydrological station, the mean annual sediment load during 1996-2006 was merely one-quarter of the long-term average [55]. This dramatic sediment reduction has been primarily attributed to changes in rainfall intensity and intensified anthropogenic activities [56, 57]. The recent implementation of large-scale vegetation restoration programs has substantially mitigated soil erosion rates. However, as the sediment trapping capacity of existing dams and reservoirs gradually diminishes in the future, the erosion rates across the Loess Plateau will increasingly determine the sediment flux in the Yellow River [58]. These research findings collectively corroborate the results of the present study, providing a comprehensive explanation for the hydrological processes governing the Yellow River's water-sediment regime.

Combined with these findings from related studies in this area, indicating increased vegetation coverage in this region, both runoff and sediment load have exhibited significant downward trends [57-59]. While efforts to restore vegetation in the Middle Yellow River Basin have effectively diminished soil erosion, the process has also resulted in an increase in water consumption. This is predominantly because precipitation levels have remained relatively stable, thereby intensifying the demand for water resources required to sustain the restored vegetation. Consequently, this heightened water usage could potentially elevate the risks associated with regional water ecological security.

Conclusions

Based on precipitation data from 15 stations in the middle reaches of the Yellow River, this study analyzes the spatiotemporal variation characteristics of precipitation in the region. The main findings are as follows:

- (1) Trend and abrupt change analysis of annual precipitation from 1956 to 2022 reveals an overall declining trend, though not statistically significant, with increasing precipitation in the northeastern and northern areas and decreasing precipitation in the southwestern and southern regions. Abrupt changes in annual precipitation were detected in Long, Zhengzhou, and Taiyuan around 1978, 2003, and 2020. Regional annual precipitation series exhibited no statistically significant mean shifts.
- (2) Periodicity analysis indicates three dominant time scales across the study area: 5-10 years, 15-30 years, and 30-55 years. Stations such as Hohhot, Jiexiu, and Sanmenxia exhibit more pronounced cycles at 5-10,

- 15-25, and 35-50 years, consistent with the pattern of increasing wavelet variance energy from shorter to longer time scales. The most significant periodicities were identified at 10, 44, and 56 years.
- (3) Spatial heterogeneity tests on 67 years of precipitation data demonstrate that differences in precipitation are closely associated with inter-station distance and latitude. Stations in close proximity or at similar latitudes show no significant differences, whereas those farther apart or at differing latitudes exhibit significant disparities.
- (4) The global Moran's I (I = 0.5533, p<0.05) confirms a significant positive spatial autocorrelation in annual precipitation across the region. Local Moran's I analysis reveals high-high clustering (indicating abundant rainfall) in the southern part, low-low clustering (indicating rainfall scarcity) in the northern and southwestern areas, and nonsignificant spatial patterns in the central region.

This study enhances the understanding of hydrological cycle processes in the Yellow River Basin and provides a theoretical foundation for the efficient utilization of water resources in the region. Additional methodological approaches and a more detailed exploration of precipitation—environment interactions are warranted; integrating these dimensions will form the focus of our subsequent work.

Acknowledgements

This research was funded by the Key Natural Science Research Project of Anhui Provincial Department of Education (2023AH051587); the Initial Scientific Research Fund Project of Chuzhou University (2022qd002); Anhui Provincial Undergraduate Innovation and Training Program (2024CXXL036).

Conflict of Interest

The authors declare no conflict of interest.

References

- PRAVEEN B., TALUKDAR S., SHAHFAHAD., MAHATO S., MONDAL J., SHARMA P., REZA A., ISLAM T., RAGMAN A. Analyzing trend and forecasting of rainfall changes in India using non-parametrical and machine learning approaches. Scientific Reports. 10 (1), 10342, 2020.
- LUO M., PAN C., ZHAN C. Diagnosis of change in structural characteristics of streamflow series based on selection of complexity measurement methods: Fenhe River Basin, China. Journal of Hydrologic Engineering. 24 (2), 05018028, 2019.
- YANG W.X., YANG Y.P., CHEN Z.L., GU Y.X. Systemic Impacts of National Civilized Cities on Sustainable Development: A Quasi-Experimental Analysis of

- Economic and Environmental Outcomes in China. Systems. 13 (1), 23, 2025.
- 4. ZHANG W.X., ZHOU T.J., YE W.H., ZHANG T.Y., ZHANG L.X., WOLSKI P., RISBEY J., WANG Z., MIN S., RAMSAY H., BRODY M., GRIMM A., CLARK R., REN K., JIANG J., CHEN X., FU S., LI L., TANG S., HU S. A year marked by extreme precipitation and floods: Weather and climate extremes in 2024. Advances in Atmospheric Sciences. 42 (6), 1045, 2025.
- ZEPPEL M., WILKS J., LEWIS J. Impacts of extreme precipitation and seasonal changes in precipitation on plants. Biogeosciences. 11, 3083, 2014.
- FENG J.M., DONG B.Q., QIN T.L., LIU S.S., ZHANG J.W., GONG X.F. Temporal and Spatial Variation Characteristics of NDVI and Its Relationship with Environmental Factors in Huangshui River Basin from 2000 to 2018. Polish Journal of Environmental Studies. 30 (4), 3043, 2021.
- FU J., JIAN Y.W., WANG X.H., LI L., CIAIS P., ZSCHEISCHLER J., WANG Y., TANG Y., MULLER C., WEBBER H. Extreme rainfall reduces one-twelfth of China's rice yield over the last two decades. Nature Food. 4 (5), 416, 2023.
- 8. ZHANG Q., SUN P., SINGH P., CHEN X.H. Spatial-temporal precipitation changes (1956–2000) and their implications for agriculture in China. Global and Planetary Change. 82, 86, 2012.
- LIU J.J., ZHAO Y.L., LIU W. Impact of climate extremes on agricultural water scarcity and the spatial scale effect. Frontiers of Agricultural Science and Engineering. 11 (4), 515, 2024.
- ZHAO Q., LIU X., WU Y., LIU H., QU F., ZHANG M. Impact of the eastern Tibetan Plateau on the ecological sensitivity of the West Qinling Mountains. Scientific Reports. 15 (1), 4970, 2025.
- ZHENG S.Y., CHEN J.W., QIAO J.B., PAN X.T., XU X.J., ZHANG L., LIU G.H., GU X.C. Analysis of Water-Sand Changes and Influencing Factors in the Ganjiang River Basin from 1958-2019. Polish Journal of Environmental Studies. 33 (2), 1949, 2024.
- 12. EASTERLING R., KUNKEL K., ARNOLD J., KNUTSON T., LEGRANDE A., LEUNG L., VOSE R., WALISER D., WEHNER M. Precipitation change in the United States. In: Climate Science Special Report: Fourth National Climate Assessment, Volume I Wuebbles D., Fahey D., Hibbard K., Dokken D., Stewar B., Maycock T., (eds.), U.S. Global Change Research Program, Washington, USA, pp. 207-230, 2017.
- 13. DU J.K., QIU Y.Q., LI Y.L., LU Q., HAO C.F., LIU H.Y. Evolution characteristics of the interannual and intraannual precipitation in China from 1956 to 2016. Advances in Water Science. **34** (2), 182, **2023**.
- CHEN Y., MA L., LIU T.X., HUANG X., SUN G.H. Spatio-Temporal Variation Characteristics of Summer Precipitation in China and Its Response to ENSO. Polish Journal of Environmental Studies. 32 (6), 4981, 2023.
- LI L., NI J.R., CHANG F., YUE Y., FROLOVA N., MAGRITSKY D., BORTHWICK A., CIAIS P., WANG Y., ZHENG C., WALLING D.E. Global trends in water and sediment fluxes of the world's large rivers. Science Bulletin. 65 (1), 62, 2020.
- 16. YANG W.X., ZHENG X., YANG Y.P. Impact of environmental regulation on export technological complexity of high-tech industries in Chinese manufacturing. Economies. 12 (2), 50, 2024.

- KONG D., MIAO C., GOU J., ZHANG Q., SU T. Sediment reduction in the middle Yellow River basin over the past six decades: Attribution, sustainability, and implications. Science of the Total Environment. 882, 163475, 2023.
- 18. HOU B.F., JIANG C., SUN O. Differential changes in precipitation and runoff discharge during 1958–2017 in the headwater region of Yellow River of China. Journal of Geographical Sciences. 30, 1401, 2020.
- WANG K., ZHOU J., TAN M., LU P., XUE Z., LIU M., WANG X. Impacts of vegetation restoration on soil erosion in the Yellow River Basin, China. Catena. 234, 107547, 2024
- YANG L.F., LIU J.H., YANG W.X. Impacts of the sustainable development of cross-border e-commerce pilot zones on regional economic growth. Sustainability. 15 (18), 13876, 2023.
- 21. ZHANG K.L., FANG B., ZHANG Z.C., LIU T., LIU K. Exploring future ecosystem service changes and key contributing factors from a "past-future-action" perspective: A case study of the Yellow River Basin. Science of The Total Environment. 926, 171630, 2024.
- HUANG J., ZHONG P.S., ZHANG J.Z., ZHANG L. Spatial-temporal differentiation and driving factors of ecological resilience in the Yellow River Basin, China. Ecological Indicators. 154, 110763, 2023.
- 23. GAO M.M., YANG N., LIU Q. What Drives Vegetation Evolution in the Middle Reaches of the Yellow River Basin, Climate Change or Human Activities? Sustainability. 16 (22), 10122, 2024.
- 24. WANG L.M., XUE W.X. Research on Synergistic Development between Environment and Industry in the Yellow River Basin. Polish Journal of Environmental Studies. 33 (5), 5303, 2024.
- HAN Y., ZHAO L. Trend Analysis of Rainfall Erosivity in Liaoning Province (2003-2022) using the Mann-Kendall Test. E3S Web of Conferences. Vol. 630. EDP Sciences. 2025.
- 26. DAS S., BANERJEE S. Investigation of changes in seasonal streamflow and sediment load in the Subarnarekha-Burhabalang basins using Mann-Kendall and Pettitt tests. Arabian Journal of Geosciences. 14 (11), 946, 2021.
- OSTERTAGOVA E., OSTERTAG O., KOVAC J. Methodology and application of the Kruskal-Wallis test. Applied Mechanics and Materials. 611, 115, 2014.
- 28. YAN J., WANG X.Y., WANG T., ZHENG X., Research on the Spatiotemporal Evolution and Influencing Factors of Sudden Environmental Incidents in China from 2008 to 2021. Polish Journal of Environmental Studies. 34 (1), 2025.
- 29. LIU X., YANG X., CUI G., LIU Y., YANG W., QU X.N., WANG L., TONG S.Z. Hydrometeorological variation in the middle and upper reaches of the Yellow River Basin (1960-2019). HydroResearch. 7, 32, 2024.
- LIU Q., YANG Z.F., CUI B.S. Spatial and temporal variability of annual precipitation during 1961–2006 in Yellow River Basin, China. Journal of Hydrology. 361 (3-4), 330, 2008.
- CHANG J.X., WEI J., WANG Y.M., YUAN M., GUO J.C. Precipitation and runoff variations in the Yellow River Basin of China. Journal of Hydroinformatics. 19 (1), 138, 2017.
- 32. WANG M.Y., CHEN Y.B., LI J.Y., ZHAO Y.J. Spatiotemporal evolution and driving force analysis of drought characteristics in the Yellow River Basin. Ecological Indicators. 170, 113007, 2025.

- 33. LV Z.Y., QIN T.L., WANG Y., MU J.X., LIU S.S., NIE H.J. Effects of Recent and Potential Land Use and Climate Changes on Runoff and Sediment Load in the Upper Yellow River Basin, China. Polish Journal of Environmental Studies. 29 (6), 4225, 2020.
- 34. ABBAS A., HUANG P., HUSSAIN S., SHEN F., WANG H., DU D. Mild Evidence for Local Adaptation of Solidago canadensis under Different Salinity, Drought, and Abscisic Acid Conditions. Polish Journal of Environmental Studies. 31 (4), 2987, 2022.
- CABRAL J., LUCENA L. Analysis of precipitation using Mann-Kendall and Kruskal-Wallis non-parametric tests. Mercator (Fortaleza). 19, e19001, 2020.
- 36. XU M.Z., WANG G.H., WANG Z.J., HU H.C., SINGH D. K., TIAN S.M. Temporal and spatial hydrological variations of the Yellow River in the past 60 years. Journal of Hydrology. 609, 127750, 2022.
- WU L., LIU X., MA X.Y. Spatio-temporal evolutions of precipitation in the Yellow River basin of China from 1981 to 2013. Water Science and Technology: Water Supply. 16 (5), 1441-1450, 2016.
- 38. QIAN W.H., QIN A. Precipitation division and climate shift in China from 1960 to 2000. Theoretical and Applied Climatology. 93, 1, 2008.
- LU Y.J., JIANG S.H., REN L.L., ZHANG L.Q., WANG M.H., LIU R.L., WEI L.Y. Spatial and temporal variability in precipitation concentration over mainland China, 1961– 2017. Water. 11 (5), 881, 2019.
- XU Z.X., LI J.Y., LIU C.M. Long-term trend analysis for major climate variables in the Yellow River basin. Hydrological Processes: An International Journal. 21 (14), 1935, 2007.
- MU L., FANG L., DOU W.B., WANG C.C., QU X.J., YU Y.C. Urbanization-induced spatio-temporal variation of water resources utilization in northwestern China: A spatial panel model based approach. Ecological Indicators. 125, 107457, 2021.
- 42. HAN Z.Q., ZUO Q.T., WANG C.Q., GAN R. Impacts of climate change on natural runoff in the Yellow River Basin of China during 1961-2020. Water. 15 (5), 929, 2023.
- CHEN L., YANG M.X., LIU X., LU X. Attribution and sensitivity analysis of runoff variation in the yellow river basin under climate change. Sustainability. 14 (22), 14981, 2022.
- 44. CAO J.X., ZHANG M.M., CHEN E.Q. The Dynamic Effects of Ecosystem Services Supply and Demand on Air Quality: A Case Study of the Yellow River Basin, China. Polish Journal of Environmental Studies. 2025.
- 45. FENG Y.J., ZHU A.K. Spatiotemporal differentiation and driving patterns of water utilization intensity in Yellow River Basin of China: Comprehensive perspective on the water quantity and quality. Journal of Cleaner Production. 369, 133395, 2022.
- 46. WANG B.L., WANG H.X., JIAO X.Y., HUANG L.T., CHEN H., GUO W.X. Runoff change in the Yellow River Basin of China from 1960 to 2020 and its driving factors. Journal of Arid Land. 16 (2), 168, 2024.

- 47. ZHAO G.L., TIAN S.M., JING Y.C., LIANG S., WANG W.W., CHEN R.X., ZHANG Y. Spatiotemporal variations in runoff and sediment load of the mainstem and major tributaries of the Yellow River Basin from the headwater to the estuary (1960-2023). Journal of Environmental Management. 380, 124723, 2025.
- 48. WANG S.Y., LIU J.S., MA T.B. Dynamics and changes in spatial patterns of land use in Yellow River Basin, China. Land Use Policy. 27 (2), 313, 2010.
- JIANG W.G., YUAN L.H., WANG W.J., CAO R., ZHANG Y.F., SHEN W.M. Spatio-temporal analysis of vegetation variation in the Yellow River Basin. Ecological Indicators. 51, 117, 2015.
- 50. HUANG Y.L., JIN Y.X., CHEN S. The Spatiotemporal Dynamics of Vegetation Cover and Its Response to the Grain for Green Project in the Loess Plateau of China. Forests. 15 (11), 1949, 2024.
- ZHANG B., GUO J.L., FANG H.Y., WU S.F., FENG H., SIDDIQUE K. Soil erosion projection and response to changed climate and land use and land cover on the Loess Plateau. Agricultural Water Management. 306, 109187, 2024.
- 52. FENG X.M., FU B.J., PIAO S.L., WANG S., CIAIS P., ZENG Z.Z., LV Y.H., ZENG Y., LI Y., JIANG X., WU B. Revegetation in China's Loess Plateau is approaching sustainable water resource limits. Nature Climate Change. 6 (11), 1019, 2016.
- 53. CHEN Y., WANG K., FU B., WANG Y., TIAN H., WANG Y., ZHANG Y. 65% cover is the sustainable vegetation threshold on the Loess Plateau. Environmental Science and Ecotechnology. 22, 100442, 2024.
- 54. SHI L., YANG L.Y., XIA L.H., ZHANG P.P., SUN Z.H. Temporal and Spatial Distribution of Gully Water and its Replenishment Pathways in Loess Plateau. Polish Journal of Environmental Studies. 34 (3), 2835, 2025.
- LIU C., SUI J., WANG Z. Changes in Runoff and Sediment Yield along the Yellow River during the Period from 1950 to 2006. Journal of Environmental Informatics. 12 (2), 129, 2008.
- 56. XU J., JIANG X., SUN H., XU H., ZHONG X., LIU B., LI L. Driving forces of nature and human activities on water and sediment changes in the middle reaches of the Yellow River in the past 100 years. Journal of Soils and Sediments. 21 (6), 2450, 2021.
- 57. SHI H., HU C., WANG Y., LIU C., LI H. Analyses of trends and causes for variations in runoff and sediment load of the Yellow River. International Journal of Sediment Research. 32 (2), 171, 2017.
- ZHAO Y., HU C., ZHANG X., LV X., YIN X., WANG Z. Response of sediment discharge to soil erosion control in the middle reaches of the Yellow River. Catena. 203, 105330, 2021.
- WANG H., SUN F. Variability of annual sediment load and runoff in the Yellow River for the last 100 years (1919-2018). Science of the Total Environment. 758, 143715, 2021.